Journal of Civil Structural Health Monitoring (2019) 9:597–605
https://doi.org/10.1007/s13349-019-00351-w

ORIGINAL PAPER

Dynamic response measurement of steel plate structure utilising video camera method

Sakhiah Abdul Kudus[1] · Kunitomo Sugiura[2] · Yasuo Suzuki[3] · Masahide Matsumura[2]

Received: 27 December 2018 / Accepted: 14 August 2019 / Published online: 24 October 2019

Abstract
Vibration measurement is a common method used to assess a structure's condition. The basic premise for the detection of damage in a structure is based on vibration measurement, whereby changes of stiffness, vibration mode, and energy dissipation in the system can cause changes in the dynamic response. The vibration measurement is conducted by obtaining the fundamental period to judge the health condition of the monitored structure. This research used the high-speed camera (HSC) to capture the structure motion during the vibration of steel-plated structure. Laboratory experiments were performed on a thin steel plate ($600 \times 600 \times 2.3$ mm) and orthotropic steel deck. The HSC was used to measure the resonance frequency of the structure monitored.

Keywords Vibration measurement · High-speed camera · Steel structure

1 Introduction

Structure deterioration due to poor maintenance, especially steel structures may lead to the loss of structures that are worth thousands of dollars. One of the examples is steel sheet pile which acts as a retaining wall in quays, harbours, and river revetment structures. Generally, the assessment of structures is quite challenging due to the limited access to the structure. Without proper preservation of the existing structures, more money will be lost. Thus, there is the need for damage assessment. Accurate detection and characterisation of damage in the monitored structure can provide information which are useful in developing maintenance strategy and remedial plan. Structural health monitoring (SHM) and non-destructive testing (NDT) are two main categories of techniques to assess and determine the health condition of the structure.

✉ Sakhiah Abdul Kudus
sakhiah@uitm.edu.my

[1] Faculty of Civil Engineering, Universiti Teknologi MARA, 40450 Shah Alam, Selangor, Malaysia

[2] Department of Civil and Earth Resources Engineering, Graduate School of Engineering, Kyoto University, Kyoto 615-8540, Japan

[3] Department of Civil Engineering, Faculty of Sustainable Design, University of Toyama, Toyama 930-8555, Japan

Most of the literature utilised the changes in measured vibration response for damage assessment and identification due to the presence of structural damage that leads to the alteration in vibration characteristics, namely natural frequency, mode shapes, and modal damping [1–4]. SHM is a technique used to determine the damage by observing changes in vibration modes [5, 6]. The general SHM system usually comprised of detection, monitoring, and assessment of any event that may affect the health state of the structure globally. On the other hand, NDT can be described as a non-invasive technique used to examine test object, component, or structure without disturbing the usefulness of the feature [7]. NDT is typically used to locate and evaluate any damage or changes in the local area [8, 9].

There are various established methods used in experimental testing to conduct vibration measurement. The common method used is the attachment of contact sensors such as strain gauges and accelerometers on the structure [10, 11]. Accelerometers are promising instruments that provide precise measurement. However, this method can only provide users with local point-wise information. It is impractical to attach thousands of sensors over a large monitored region. Conventional sensors can distribute the numbers of wiring in increasing setup time and contributing noise during the measurement. The information on deformation's distribution cannot be obtained using these methods.

To overcome the limitation of the contact method, there were extensive research on the feasibility of non-contact techniques for vibration measurement. The emergence of non-contact measurement technologies had improved the accuracy of structural assessment. Accurate vibration measurement is useful in providing a more accurate damage assessment of the monitored structure. The application of Laser Doppler Vibrometers (LDV) can be used on real-scale structures for vibration monitoring [12, 13]. The LDV was also used to measure the velocity and displacement of the targeted structure from the frequency shift of reflected light. The application of LDV provides users with good accuracy using its higher resolution. However, this technique requires the structure's surface in becoming sufficiently reflective to achieve good measurements. Another method used for the measurement without making contact with the vibrated structure is speckle photography [14]. The Fourier transform is applied in electronic speckle photography. The digital holography interferometry was applied by Valin et al., to determine the micro-displacement of a square section steel bar [15]. The displacement of the specimen is conducted in air and submerged in water. The remote measurement technique can analyse the structural behaviour from the obtained displacement data.

Vibration measurement using video camera has lately received significant attention. Video camera measurement is advantageous for the measurement of the structure's response mainly at complex, inaccessible, and unreachable region of the structure. One of the examples is its application on marine structures where structure deteriorations are very common.

The application of camera for vibration measurement has been extensively conducted to measure the deformation of large scale infrastructure through the measurement of surface geometry, displacement, and strain [16–18]. The full-field measurement provided by digital camera is cost effective compared to the LDV method [19]. However, the optical technique has shortcomings, mainly in the accuracy of measuring small displacements. The smaller amplitude of vibrations also limits the vibration measurement using this technique. More attention should be given to the noise which has a significant disturbance to the structural response, if the noise frequency of the system is higher or close to the frequency of the vibrating structure. Higher resolution-based measurement offers significant improvement over the current practices.

There was lack of research in the utilisation of camera for vibration analysis. The present study aimed to investigate the performance and accuracy of the optical measurement aided by HSC for vibration measurement on the surface of the steel structure. The results revealed that the optical measurement with the HSC is one of the approaches to obtain resonance frequency of the monitored structure.

2 Image analysis

2.1 Correlation method

The image analysis by digital image correlation (DIC) is a technique used for the determination of displacement and displacement gradient based on the comparison of two video images captured before and after the deformation [20]. The fundamental of this technique is best described as the movement of the pixel within a region of interest to another location based on the changes in the intensity of pixel's grayscale [21]. Figure 1 presents the schematic diagram of the basic principle of a two-dimensional DIC system. Generally, the DIC software uses the first image in a series as the reference image and the displacements for each consecutive image in the sequence are calculated based on the first reference frame [21]. Based on this principle, the computations of the displacement in each pixel or region of interest are possible for each image.

This research adopted motion analysis software, MoviasNeo to perform image tracking and extract the movement of targeted points. Several parameters need to be specified before image analysis including the subset size. The subset size is highly associated with the quality of subset image. A larger subset size can reduce the accuracy and lead to incorrect approximation, whereas smaller subset size can result in lower image quality [22]. Several subset sizes were defined to obtain optimum result. The subset size was varied from 9×9 pixel^2 to 20×20 pixel^2. In the analysis from experiment 1, it was observed that the results from the larger subset size of 12×12 pixel^2 were closest to the conventional methods. However, it depends on the resolution of the camera.

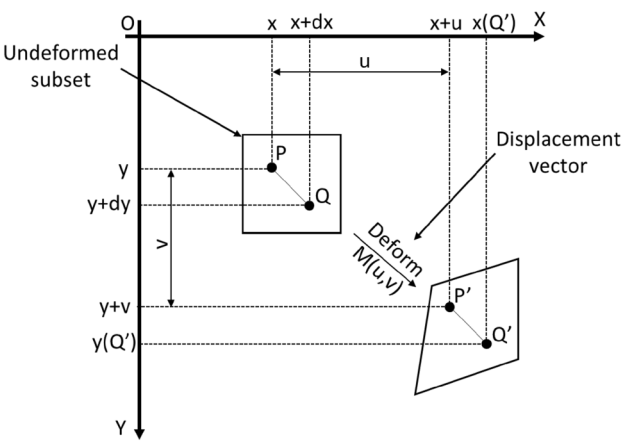

Fig. 1 Schematic diagram of subset before and after deformation [21]

2.2 Two-dimensional camera setup

The experimental setup for optical measurement by the HSC does not require a complex system. However, the instrumentation setup is important to warrant the accuracy and consistency of the results [21]. For experiment 1, random speckle patterns were sprayed on the measurement region surface to provide grey-scale distribution with sufficient contrast in enabling the tracking from image to image when capturing the deformation of tested specimen. The pattern is made as thin as possible. The average size of speckles and their distribution in the random pattern play an important role. Bruck et al. used coarse–fine search method to correlate the images and found that the size of the speckle should be in two to three pixel's size to achieve satisfactory correlation results [20]. For experiment 2, image tracking is conducted from the mark point made on the surface of the region.

Figure 2 shows a schematic diagram of the test setup. This arrangement represents the two-dimensional (2D) camera setup which allows the measurement of in-plane deformation. The camera is placed perfectly parallel to the measurement region before adjusting the distance. LED light sources were employed to illuminate the targeted region in minimising light disturbance from the surrounding testing area. The HSC data were synchronised with the measurements by strain gauges. The camera has to be calibrated before proceeding to the testing. The planar calibration method is commonly used in combining the intrinsic and extrinsic parameters of the camera simultaneously [23]. The calibration also allows the transformation from image to coordinate into geometric coordinate while maintaining the data accuracy.

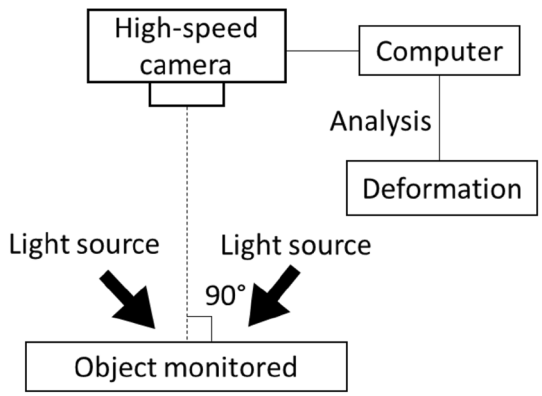

Fig. 2 Schematic diagram of test setup

3 Experiment vibration test 1

In the first experiment, the boundary condition of the plate was set as all sides are simply supported and the plate was subjected to out-of-plane harmonic excitation. The vibrator was used as a local excitation source on the flat plate steel structure. The excitation was applied at two different positions as shown in Fig. 3. The vibrator can produce mechanical impedance which is the force required to produce the desired motion on the specimen.

The HSC used in this research is the product of NAC Image Technology, namely MEMRECAM HX-7s. The camera has a maximum speed of 200,000 frames per second with the highest resolution up to 2560 × 1920 which is equivalent to 4,915,200 points of pixels. In experiment 1, the motion of the plate was recorded at 10,000 frames per second at the resolution of 640 × 592. Figure 4 shows the setup of the instrument with the object being monitored which is a steel plate with dimensions of 600 mm × 600 mm with an intact thickness of 2.6 mm. A strain gauge was mounted at the centre of the steel plate to validate the strain measurement from the camera.

The resonance frequency of the plate was determined using theoretical calculation and finite element method (FEM). The plate model was constructed using a three-dimensional FEM with a commercial FEM package called Abaqus, version 6.14. This research performed Eigenvalue analyses to obtain the natural frequencies and mode shapes. The Lanczos eigensolver in Abaqus was chosen in this analysis to solve the matrices. The following are the material properties of the steel in this research: density, $\rho = 7850$ kg/m^3; Poisson's ratio, $\nu = 0.3$; and Young's modulus, $E = 210$ GPa. The plate was modelled using S4R elements, which are four-node conventional shell elements

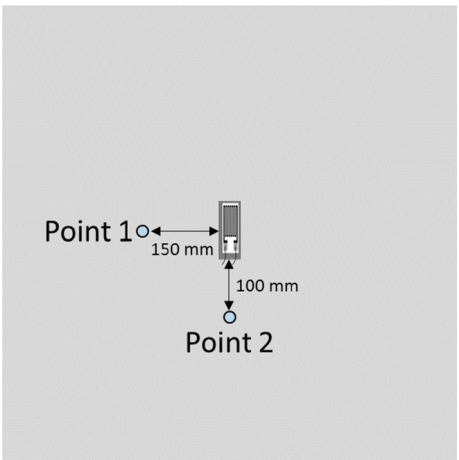

Fig. 3 The location of the excitation, Point 1 and Point 2 on steel plate

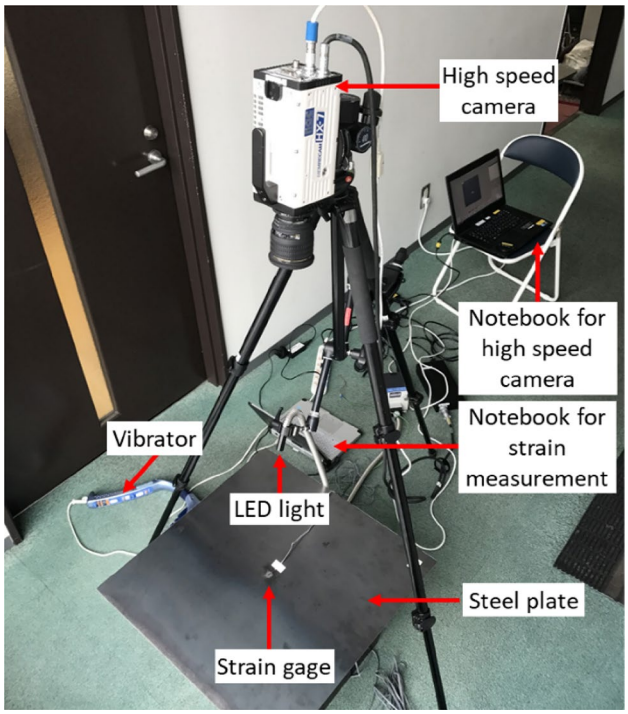

Fig. 4 The complete setup of the instrument

Table 1 The natural frequency of plate by FEM and theoretical equation

Mode number	FEM (Hz)	Theoretical by Eq. 1 (Hz)
1	31.42	31.42
2	78.55	78.54
3	78.55	78.54
4	125.66	125.66
5	157.14	157.08
6	157.14	157.08

with reduced integration. Uniform size of elements of 5 mm was used and the boundary conditions were set as a simple support for all edges of the plate as the experiment setup.

Table 1 presents the natural frequency results for the specimen which is monitored from FEM and theoretical values computed using Eq. 1 [24]. In Eq. 1, D is the flexural stiffness; ρ is the density of the plate; h is the thickness of the plate; ω is the natural frequency; and a and b are the length and width of the plate. The mode shape of the first six resonance frequency is depicted in Fig. 5. There is a good agreement between the FEM and the theoretical equation for the obtained frequency.

The mode shape describes the pattern in which the plate vibrates on its own natural frequency. In the first mode shape of vibration for $m=1$ and $n=1$, the vibration occurs in the whole plate, which causes the plate to move up and down regardless of the aspect ratio. Modes 2 and 3 of square plate have an identical mode shape pattern where two independent regions of vibration are separated by a nodal line in the middle of the plate. In mode 4, there are four independent regions that vibrate alternately up and down. Furthermore, modes 5 and 6 are also described as identical modes with nearly equal values of natural frequency but different patterns of vibration. Both modes 1 and 5 show that the vibration is dominant at the centre part of the plate.

$$\omega_{mn} = \sqrt{\frac{D}{\rho h}}\left(\left(\frac{m\pi}{a}\right)^2 + \left(\frac{n\pi}{b}\right)^2\right)(m,n=1,2,\ldots,\infty). \quad (1)$$

The strain data obtained from the measurement were filtered with the cut-off frequency for a low-pass filter of 50 Hz. Javh et al. stated that the measurement conducted by optical measurement is usually burdened by noise [25]. Moreover, the displacement amplitude of the vibrating object monitored is small and it is usually in the range of micrometre, depending on the type of structure and disturbance by the noise from the camera. Figures 6 and 7 show the results of strain data for the excitation at Points 1 and 2, respectively. The data were converted to the frequency domain by fast Fourier transform (FFT). Figure 8 shows the FFT result of the strain gage data for the excitation at Point 1; while, Fig. 9 shows the frequency domain data when the excitation is applied at Point 2. The clear peak is observed at 30 Hz, 60 Hz, and 80 Hz. The 30-Hz frequency is identical to the resonance frequency for the first mode of the specimen monitored. The peak of 60-Hz frequency represents the frequency of electric supply for the vibrator during the testing and the frequency of around 80 Hz represents the second and third resonance frequency of the plate.

This section discusses the analysis from the image captured by the camera during testing. This research considered two targeted points, namely P1 and P2. P1 and P2 are located 11.73 mm apart which is equivalent to 94 pixels. Generally, the pixel size does not have a particular or specific size and the pixel size is highly dependent on the camera resolution. In this analysis, 1-pixel size is equivalent to 0.1248-mm distance apart.

The deformation on the reference points of P1 and P2 was calculated in both x- and y-directions. The strain was then computed from the deformation result. The Y-axis strain data for both cases of excitation are presented in Figs. 10 and 11. Table 2 presents the summary of strain data. The maximum and minimum strain information in time domain obtained from the HSC has a slight difference from the strain data obtained from strain gauges. However, the strain measurement from HSC has better accuracy in capturing small changes in the plate movement which is below 1 με with several decimal places. In practice, measurement using

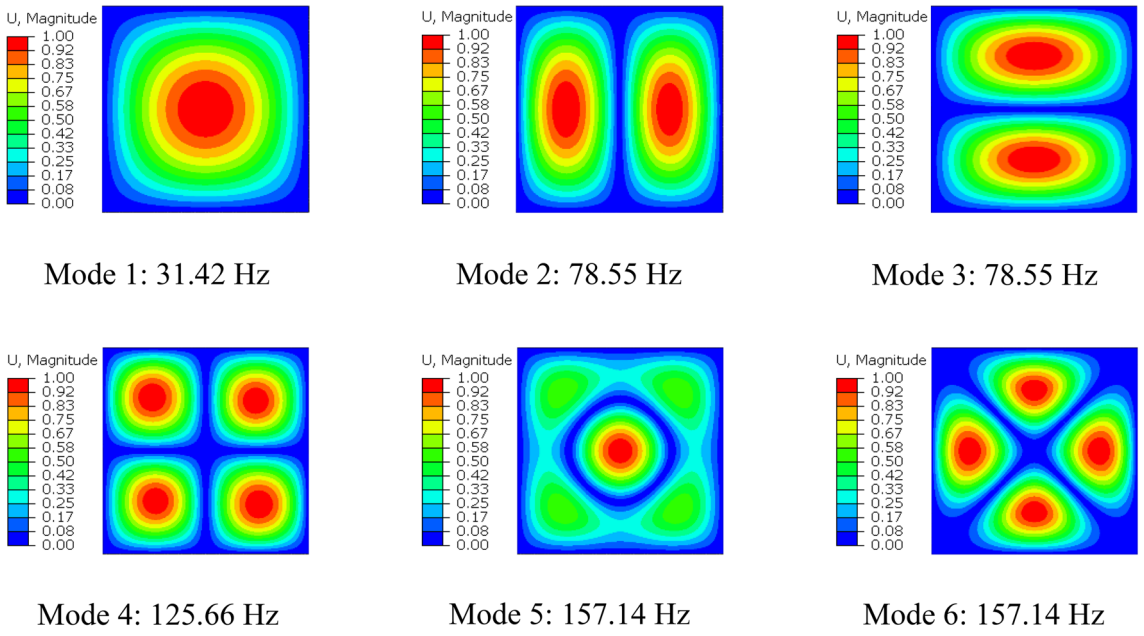

Fig. 5 The first sixth mode shape and natural frequency of intact square plate

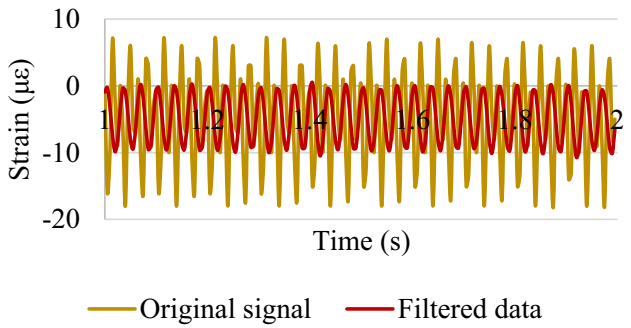

Fig. 6 The time history of strain data by strain gauge due the excitation at Point 1 for original and filtered signal

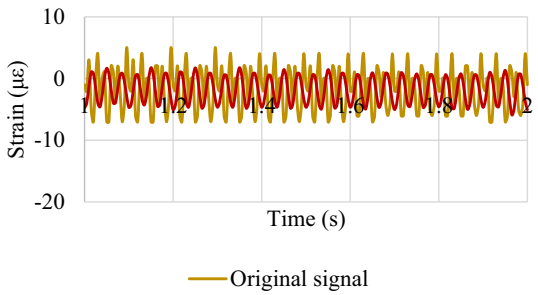

Fig. 7 The time history of strain data by strain gauge due the excitation at Point 2 for original and filtered signal

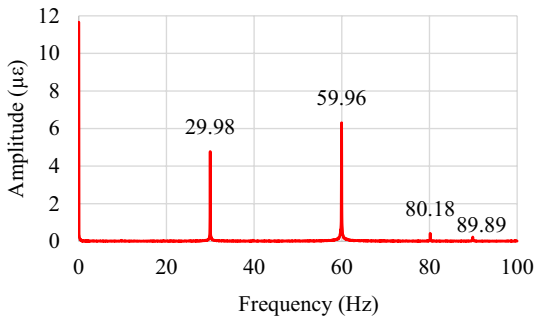

Fig. 8 The FFT of strain data by strain gauge due the excitation at Point 1

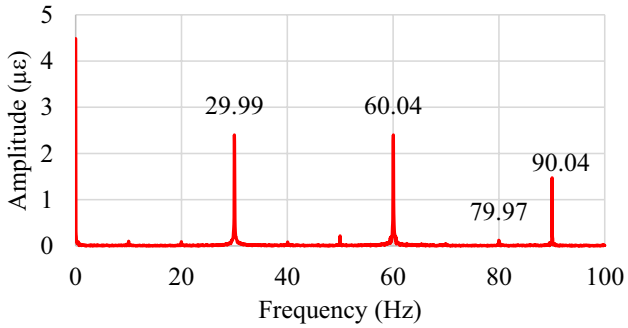

Fig. 9 The FFT of strain data by strain gauge due the excitation at Point 2

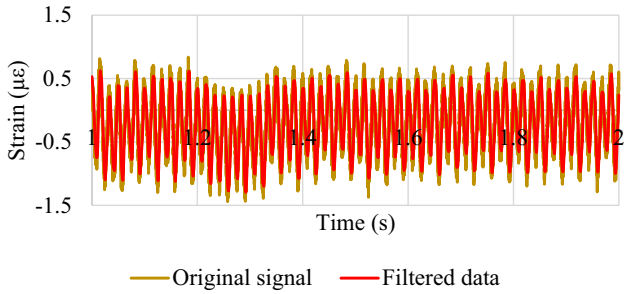

Fig. 10 The time history of strain data by HSC due the excitation at Point 1

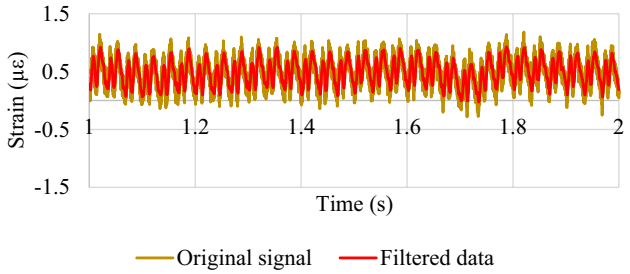

Fig. 11 The time history of strain data by HSC due the excitation at Point 2

Table 2 The minimum and maximum value of strain from HSC in *Y*-axis direction

Details	Excitation at Point 1		Excitation at Point 2	
	Strain (με)	Stress (kPa)	Strain (με)	Stress (kPa)
Maximum	0.83822	176.02	1.26699	266.07
Minimum	− 1.69372	− 355.68	− 0.38055	− 79.92

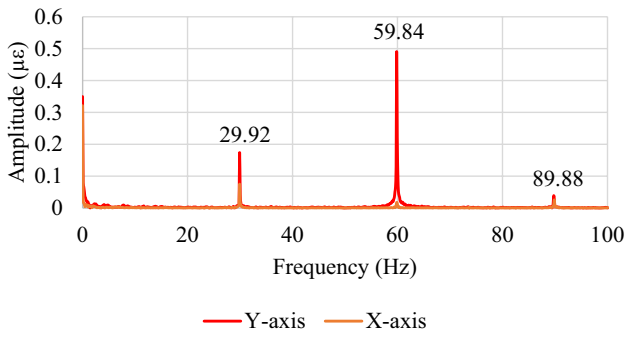

Fig. 12 The FFT of strain data by HSC due the excitation at Point 1

strain gauges is limited to capturing the minimum strain of 1 με without any decimal place. The strain data were further evaluated for frequency domain.

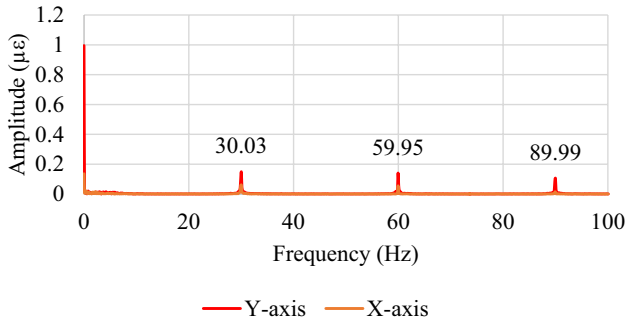

Fig. 13 The FFT of strain data by HSC due the excitation at Point 2

Table 3 Summary of peak frequency on FFT graph of strain data by two different measurement technique which is strain gauge and optical image technique

Details	Excitation at Point 1 (Hz)		Excitation at Point 2 (Hz)	
	Strain gauge	HSC	Strain gauge	HSC
Peak 1	29.98	29.95	30.03	29.68
Peak 2	59.91	59.91	60.01	59.37
Peak 3	80.13	–	79.98	–
Peak 4	89.89	89.86	90.04	89.13

Figures 12 and 13 present the frequency result for HSC at two different locations. Table 3 summarises the results of frequency data from both techniques of strain data measurement, and the data show good correlation for both methods. The resonance peak was identical when the plate was excited at different points. However, the third peak at around 80 Hz could not be identified by HSC corresponding to the amplitude of this peak which is small in the strain gauge data.

4 Experiment vibration test 2

This section summarises the vibration measurement using HSC on the part of an orthotropic steel deck model with an intact thickness of 10 mm. The plate was subjected to out-of-plane harmonic excitation using a vibrator. The frequency of excitation was set to 10 Hz. The plate was excited for about 1 min and the measurements were recorded by the HSC system. This experiment aimed to investigate the capability of HSC to capture small in-plane deformation on the vibrated steel-plated structure. The measurement setup of two-dimensional camera was adopted in allowing in-plane measurement. This test did not conduct verification by a conventional method using strain gauges because the applied load was in out-of-plane direction and the amplitude of vibration was too small.

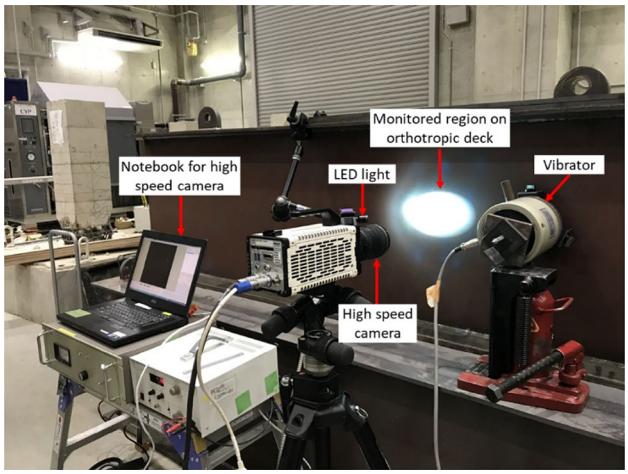

Fig. 14 The complete setup of the instrumentation used for localised vibration measurement on orthotropic steel deck

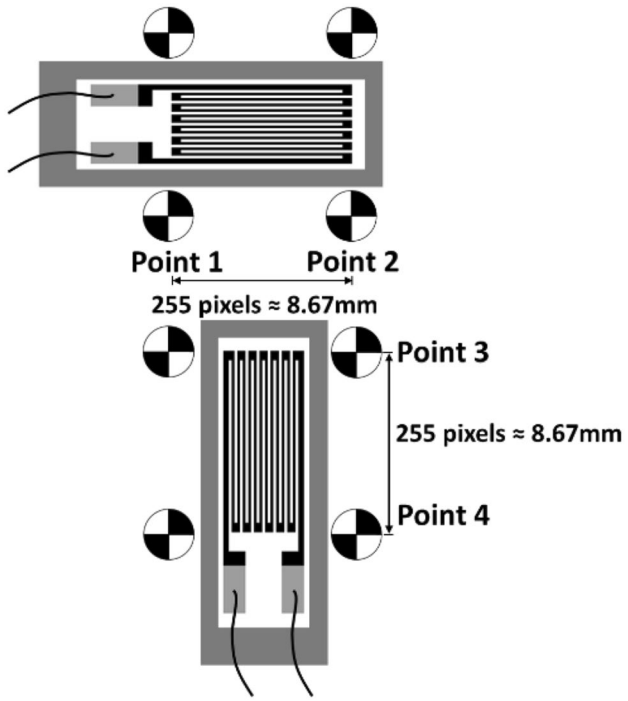

Fig. 15 The position of Point 1 and Point 2 on the orthotropic steel deck model

This experiment used the same HSC which was used in the previous experiment. In this test, the deformation of the plate was recorded at 10,000 frames per second at the resolution of 640 × 592. The camera resolutions should be sufficient to capture the spatial data on the object. The frame rate was set to track the frequency excitation on the structure. In this analysis, 1-pixel size is equivalent to 0.034 mm. Figure 14 shows the complete experimental setup for vibration measurement with HSC.

The movement of targeted points on the plate was captured and summarised for further analysis. The position of targeted points, Point 1 and Point 2 are shown in Fig. 15. Then, the displacement and strain were computed. From the data, the strain can be defined as ratio of change in length to the initial length. The results of displacement and strain were summarised in the time domain and were further converted to the frequency domain by fast Fourier transform (FFT). The results of time domain and FFT of plate excited with 10 Hz are shown in Figs. 16 and 17, respectively.

In the result for the time domain of displacement, the propagation of the harmonic wave with frequency with 10 Hz was clear. The amplitude of wave propagation was around 3.7 μm for displacement measurement at Point 1, whereas higher amplitude around 4.5 μm was obtained at Point 2. The event is explained in Fig. 18 which shows the wave propagation on the thin plate simulated by commercial finite element (FEM) software, Abaqus 6.14. The arrivals of wave packets from the source for the two different targeted points were different. Additionally, the propagation of elastic wave through the structure can interact with multiple reflections, mode conversions, and interferences of longitudinal and shear wave from the structure's boundaries.

The amplitude of the strain result was around 4.5 με in the time domain computed between Point 1 and Point 2. The amplitude obtained was larger than expected probably due to the resonance phenomena where the vibrating structure oscillated with greater amplitude at certain frequencies. The displacement and strain data were then further evaluated in terms of frequency domain. The distinct peak observed around 10 Hz represented the frequency of excitation. Overall, it can be concluded that the HSC was able to perform vibration measurements for the 10 Hz frequency of excitation.

Two strain gauges were mounted on the surface of the orthotropic steel deck model to verify the results from the HSC. Point 1 and Point 2 represented the horizontal strain gauges, whereas the Point 3 and Point 4 were used to verify the strain data from the vertical strain gauges.

5 Concluding remark

A thorough understanding of the vibration of a structure is important in resolving any vibration problems. This research conducted vibration measurements and obtained the following conclusion:

- In general practice, measurements using strain gauges are limited to capture strains above 1 με. However, it was observed that the strain measurement from HSC could

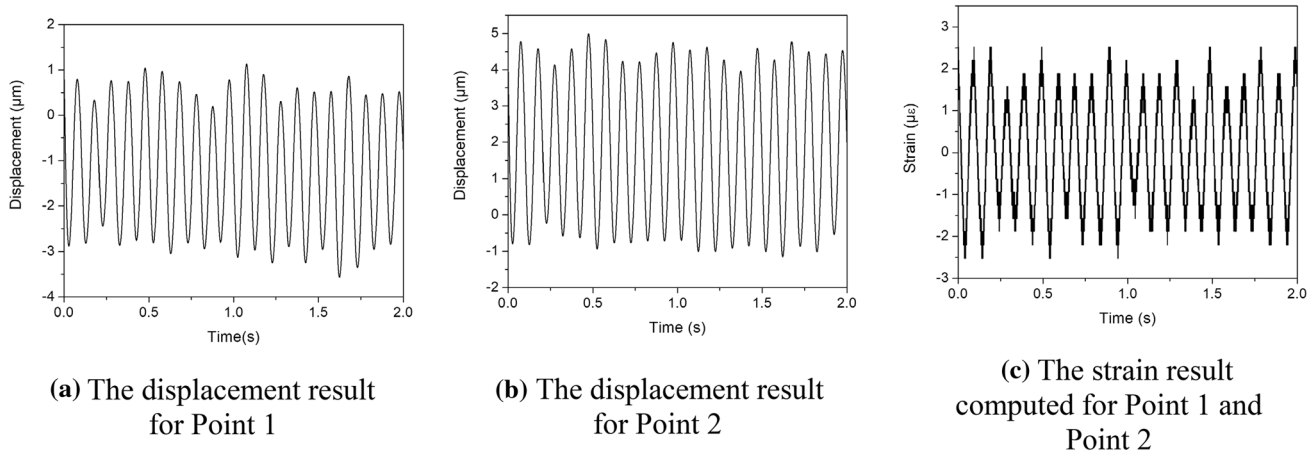

(a) The displacement result for Point 1

(b) The displacement result for Point 2

(c) The strain result computed for Point 1 and Point 2

Fig. 16 The vertical time domain response on plate excited by 10-Hz frequency

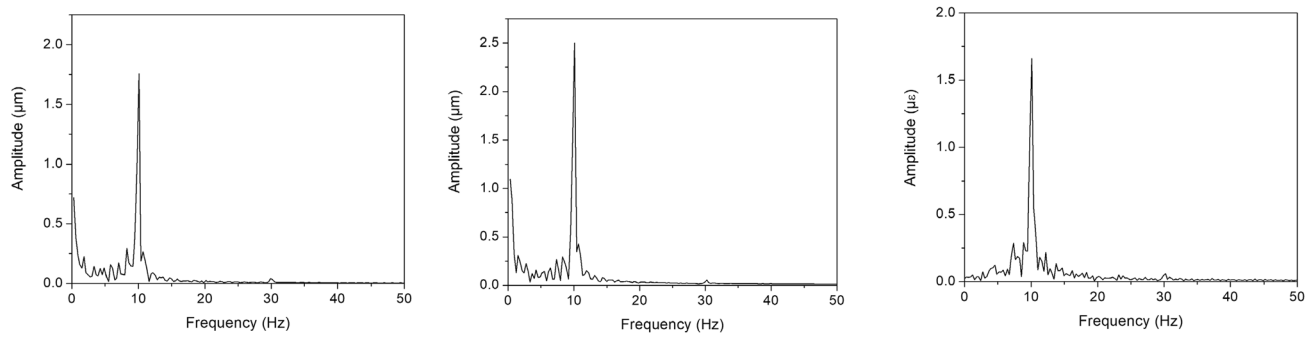

(a) The displacement result for Point 1

(b) The displacement result for Point 2

(c) The strain result computed for Point 1 and Point 2

Fig. 17 The frequency domain response on plate excited by 10-Hz frequency

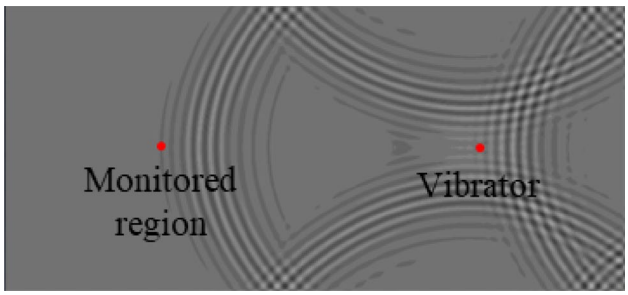

Fig. 18 The wave propagation on the thin steel plate simulated by FEM

capture measurement changes in the plate for below 1 με with several decimal places. This finding could help engineers to overcome the limitation of the current strain measurement method.

- The FFT graph showed a distinct peak at 30 Hz which represented the resonance frequency for mode 1 of the specimen. The second peak was around 60 Hz which was equivalent to the frequency of the current supply for the vibrator during the testing. The third peak was around 80 Hz which represented the second and third resonance frequencies of the plate. The results matched very well with the resonance frequency of the steel plate.
- In experiment 2, the HSC was more capable in detecting the harmonic wave which was applied to the test structure at lower frequencies. However, the measurement at higher frequencies tends to produce inconsistent amplitudes.

The strain data from strain gauge measurements and HSC measurements confirmed to have good correlation in terms of frequency measurement. Hence, the application of HSC can be optimised in the engineering field.

Acknowledgements The authors would like to express their gratitude to NAC Image Technology for providing the high-speed camera.

References

1. Carden EP, Fanning P (2004) Vibration based condition monitoring: a review. Struct Health Monit 3(4):355–377
2. Fan W, Qiao P (2011) Vibration-based damage identification methods: a review and comparative study. Struct Health Monit 10(1):83–111
3. Kudus SA, Suzuki Y, Matsumura M, Sugiura K (2018) Damage assessment based on sensitivity of modal parameter in plated structure. Malays Constr Res J 24(1):65–82
4. Salawu OS (1997) Detection of structural damage through changes in frequency: a review. Eng Struct 19(9):718–723
5. Farrar CR, Worden K (2007) An introduction to structural health monitoring. Philos Trans Royal Soc A 365(851):303–315
6. Worden K, Farrar CR, Manson G, Park G (2007) The fundamental axioms of structural health monitoring. Proc Royal Soc A 463(2082):1639–1664
7. Shull PJ (2002) Nondestructive evaluation: theory, techniques, and applications, vol 142. CRC, US
8. Basri SR, Bunnori NM, Kudus SA, Shahiron S, Jamil MNM, Noorsuhada MN (2013) Applications of acoustic emission technique associated with the fracture process zone in concrete beam: a review. Adv Mater Res 626:147–151 **(Trans Tech Publications)**
9. Bunnori N, Nor N, Jiun K, Kudus S (2016) Analysis of failure mechanisms in fatigue test of reinforced concrete beam utilizing acoustic emission. Int J Multiphysics 8(4)
10. Doebling SW, Farrar CR, Prime MB, Shevitz DW (1996) Damage identification and health monitoring of structural and mechanical systems from changes in their vibration characteristics: a literature review (No. LA-13070-MS). Los Alamos National Lab., NM
11. Farrar CR, James GH III (1997) System identification from ambient vibration measurements on a bridge. J Sound Vib 205(1):1–18
12. Kaito K, Abe M, Fujino Y (2005) Development of non-contact scanning vibration measurement system for real-scale structures. Struct Infrastruct Eng 1(3):189–205
13. Nassif HH, Gindy M, Davis J (2005) Comparison of laser Doppler vibrometer with contact sensors for monitoring bridge deflection and vibration. NDT&E Int 38:213–218
14. Yuanpeng Z, Huaning Z, Wenling Z, Hefei L (2002) Application of the fourier transform in electronic speckle photography. Exp Mech 42(1):18–24
15. Valin JL, Gonçalves E, Palacios F, Pérez JR (2005) Methodology for analysis of displacement using digital holography. Opt Lasers Eng 43:99–111
16. Baqersad J, Niezrecki C, Avitabile P (2015) Full-field dynamic strain prediction on a wind turbine using displacements of optical targets measured by stereophotogrammetry. Mech Syst Signal Process 62:284–295
17. Helfrick MN, Niezrecki C, Avitabile P, Schmidt T (2011) 3D digital image correlation methods for full-field vibration measurement. Mech Syst Signal Process 25(3):917–927
18. Nonis C, Niezrecki C, Yu TY, Ahmed S, Su CF, Schmidt T (2013) Structural health monitoring of bridges using digital image correlation. Health Monit Struct Biol Syst 2013 8695:869507 **(International Society for Optics and Photonics)**
19. Sarrafi A, Mao Z, Niezrecki C, Poozesh P (2018) Vibration-based damage detection in wind turbine blades using phase-based motion estimation and motion magnification. J Sound Vib 421:300–318
20. Bruck HA, McNeill SR, Sutton MA, Peters WH (1989) Digital image correlation using newton-raphson method of partial differential correction. Exp Mech 29(3):261–267
21. Khoo SW, Karuppanan S, Tan CS (2016) A review of surface deformation and strain measurement using two-dimensional digital image correlation. Metrol Meas Syst 23(3):461–480
22. Yaofeng S, Pang JH (2007) Study of optimal subset size in digital image correlation of speckle pattern images. Opt Lasers Eng 45(9):967–974
23. Zhang Z (2000) A flexible new technique for camera calibration. IEEE Transactions on pattern analysis and machine intelligence, 22
24. Leissa AW (1969) Vibration of plates (NASA SP 160), Gov. Printing Office, Washington
25. Javh J, Slavič J, Boltežar M (2018) High frequency modal identification on noisy high-speed camera data. Mech Syst Signal Process 98:344–351